International Journal of Engineering Research & Technology (IJERT)
ISSN: 2278-0181
Vol. 14 Issue 12 , December - 2025

Numerical Optimization of Geometric Parameters of Baffels Configuration in Shell and Tube Heat Exchanger

Sandeep Kumar
M.tech Scholar , Heat Power and Thermal Engineering
Department Of Mech. Engineering Technocrats Institute Of Technology and Science Bhopal

Dr. Ankit Goyal
HOD Department Of Mech. Engineering Technocrats Institute Of Technology and Science Bhopal

Dr. Shashi Kumar Jain
Director: Technocrats Institute Of Technology and Science Bhopal

Prof. Priyavrat Kumar
Assistant Prof. Department Of Mech. Engineering Technocrats Institute Of Technology and Science Bhopal

Abstract- Shell-and-tube heat exchangers are widely employed in industrial thermal systems; however, their performance is often limited by inefficient shell-side flow distribution associated with conventional baffle designs. In this study, a three-dimensional steady-state computational fluid dynamics (CFD) model is developed to investigate and compare the thermal performance of a shell-and-tube heat exchanger with four shell-side configurations: no baffle, conventional wavy baffle, proposed wavy-segmented baffle, and proposed half-segmented spiral baffle. Conjugate heat transfer is employed to accurately capture coupled conduction and convection phenomena within solid and fluid domains. The numerical model is validated against published literature before being applied to a parametric investigation over a range of shell-side volumetric flow rates from 2 to 8 LPM. Key performance indicators, including hot-fluid outlet temperature, overall heat transfer coefficient, effectiveness, enhancement ratio, and logarithmic mean temperature difference (LMTD), are evaluated to quantify the influence of baffle geometry and flow rate. The results demonstrate that increasing shell-side flow rate enhances heat transfer for all configurations, with the extent of improvement strongly dependent on baffle design. Compared to the no-baffle case, the proposed baffle configurations significantly intensify turbulence, improve flow redirection, and reduce thermal boundary-layer resistance. The half-segmented spiral baffle exhibits the best overall performance, achieving up to 38% enhancement in thermal performance, a maximum effectiveness of 0.85, and a substantial reduction in LMTD. The findings confirm that optimized baffle geometry combined with appropriate shell-side flow rates can markedly improve shell-side heat transfer, offering valuable guidance for the design of high-performance shell-and-tube heat exchangers.

Keywords- Shell-and-tube heat exchanger; CFD analysis; Baffle configuration; Heat transfer enhancement; Effectiveness; Conjugate heat transfer

I. INTRODUCTION

Shell-and-tube heat exchangers are among the most widely used heat transfer devices in industrial applications such as power generation, chemical processing, HVAC, oil and gas, and refrigeration, owing to their robust construction, high-pressure tolerance, and design flexibility [1]. Heat transfer in these exchangers occurs between two fluids separated by solid tube walls, preventing mixing while allowing efficient thermal energy exchange. Their performance is strongly influenced by geometric configuration, flow arrangement, material selection, and internal components such as baffles, which play a critical role in controlling shell-side flow behaviour [2].

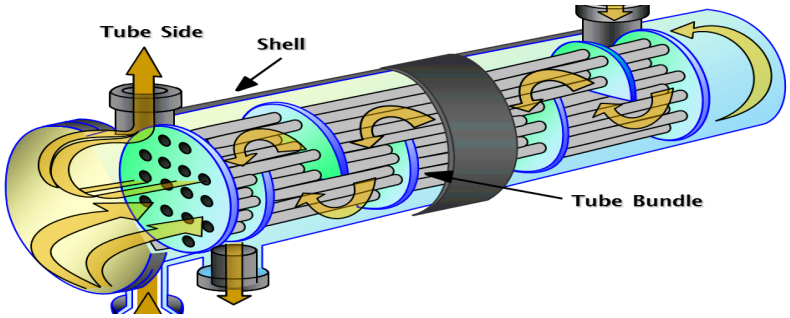

Fig. 1: Shell and Tube Heat Exchanger

International Journal of Engineering Research & Technology (IJERT)
ISSN: 2278-0181
Vol. 14 Issue 12 , December - 2025

Among the various design parameters, shell-side baffle configuration is one of the most influential factors governing heat transfer enhancement and pressure drop. Conventional segmental or wavy baffles are commonly used to induce cross-flow, increase turbulence, and suppress boundary-layer formation around tubes [3]. However, traditional baffle designs often lead to flow bypassing, dead zones, and excessive pressure losses, limiting overall thermal efficiency. Recent research has therefore focused on developing modified and hybrid baffle geometries to improve flow redirection, enhance turbulence uniformly, and achieve better thermal–hydraulic performance [4].

In this context, computational fluid dynamics (CFD) has emerged as a powerful tool for analysing complex flow and heat transfer mechanisms inside shell-and-tube heat exchangers, enabling detailed visualization of velocity, temperature, and turbulence fields that are difficult to obtain experimentally [5]. The present work employs a three-dimensional CFD approach to systematically evaluate the thermal performance of a shell-and-tube heat exchanger with no baffle, conventional wavy baffle, and newly proposed wavy-segmented and half-segmented spiral baffle configurations [6]. The study aims to quantify the effect of baffle geometry and shell-side flow rate on key performance indicators such as effectiveness, overall heat transfer coefficient, enhancement ratio, outlet temperatures, and LMTD, and to identify the most efficient baffle design for enhanced shell-side heat transfer.

II. LITERATURE REVIEW

Recent investigations on shell-and-tube heat exchangers consistently demonstrate that geometric modification of shell-side internals is an effective strategy to enhance thermal–hydraulic performance while controlling pressure losses. Advanced baffle concepts combining segmented, spiral, and multi-zonal features have been shown to improve heat transfer through enhanced turbulence and reduced dead zones, while achieving favorable trade-offs between heat transfer and pressure drop [1], [2]. CFD-based analyses further reveal that hybrid and flower-type baffle combinations significantly increase heat transfer rates (up to ~10%) with simultaneous reductions in shell-side pressure drop, resulting in measurable gains in comprehensive performance [3]. Similar numerical studies on discontinuous helical and inclined baffle arrangements confirm that flow redirection and controlled swirl intensification are key mechanisms for improving shell-side heat transfer coefficients, especially under higher Reynolds number conditions [4-6].

Beyond baffle optimization, recent studies highlight the influence of flow configuration, manufacturing methods, and optimization techniques on exchanger performance. Helically coiled and multi-pass shell configurations have achieved heat transfer improvements of 13–19% while lowering entropy generation, indicating strong potential for high-efficiency applications [7]. Multi-objective optimization and parametric studies show that geometric parameters such as baffle spacing, tube diameter ratios, and baffle count strongly affect heat transfer–pressure drop trade-offs, with optimized designs yielding over 30% improvement in performance indices [8], [9]. Continuous spiral and noncircular orifice baffle designs further enhance Nusselt numbers by 10–40% due to jet flow and pulsating vortices, though often accompanied by moderate friction penalties [10], [11]. Complementary CFD validations in industrial and food-processing applications confirm the reliability of numerical models for predicting outlet temperatures and guiding energy-efficient operation [12], while optimized helical baffle designs demonstrate balanced enhancement of heat transfer and pressure drop through evolutionary algorithms [13], [14]. Collectively, these results establish that optimized baffle geometry combined with CFD-driven analysis and optimization is central to achieving high-performance shell-and-tube heat exchangers.

III. OBJECTIVES

1. To develop a three-dimensional CFD model of a shell-and-tube heat exchanger for different baffle configurations.

2. To establish baseline thermal performance parameters using a no-baffle configuration.

3. To evaluate the thermal performance of a conventional wavy baffle design as the reference configuration.

4. To investigate the effect of newly proposed wavy segmented and half-segmented spiral baffle configurations on shell-side heat transfer.

5. To analyse the influence of shell-side volumetric flow rate on effectiveness, overall heat transfer coefficient, enhancement ratio, hot fluid outlet temperature, and LMTD.

6. To compare the thermal performance of all configurations and identify the optimal baffle design based on quantitative performance metrics.

IV. METHODOLOGY

A three-dimensional, steady-state computational fluid dynamics (CFD) model is developed to analyse the thermal performance of a shell-and-tube heat exchanger with different shell-side baffle configurations. Four configurations are investigated under identical

International Journal of Engineering Research & Technology (IJERT)
ISSN: 2278-0181
Vol. 14 Issue 12 , December - 2025

geometric and operating conditions: (i) a no-baffle configuration serving as the baseline case, (ii) a conventional wavy baffle as the reference design, (iii) a newly proposed wavy-segmented baffle, and (iv) a newly proposed half-segmented spiral baffle. The analysis focuses on quantifying the influence of baffle geometry and shell-side volumetric flow rate, varied from 2 to 8 LPM, on heat transfer performance.

Governing Equations

The fluid flow and heat transfer are governed by the following conservation equations:

Continuity Equation (Mass Conservation)

$$\nabla \cdot (\rho \mathrm{u}) = 0 \quad (1)$$

where
ρ is the fluid density and

u is the velocity vector.

Momentum Equation (Navier–Stokes Equation)

$$\nabla \cdot (\rho \mathrm{uu}) = -\nabla p + \nabla \cdot [\mu(\nabla \mathrm{u} + \nabla \mathrm{u}^T)] + \rho \mathrm{g} \quad (2)$$

where
p is the static pressure,

μ is the dynamic viscosity, and

g is the gravitational acceleration vector.

Energy Equation (Fluid Region)

$$\nabla \cdot (\rho c_p \mathrm{u} T) = \nabla \cdot (k \nabla T) \quad (3)$$

where
c_p is the specific heat capacity,

T is the temperature, and

k is the thermal conductivity of the fluid.

Energy Equation (Solid Region – Conduction)

$$\nabla \cdot (k_s \nabla T_s) = 0 \quad (4)$$

where:
k_s is the thermal conductivity of the solid and

T_s is the solid temperature.

Conjugate heat transfer (CHT) is enabled to account for the coupled heat conduction through solid regions (tubes, shell, and baffles) and convection within the fluid domains. The CFD formulation solves the governing conservation equations of mass (continuity), momentum (Navier–Stokes), and energy for the fluid region, along with a separate solid energy conduction equation. Turbulence effects are modelled using the standard k–ε turbulence model, which effectively captures turbulence-enhanced mixing and flow redirection induced by baffle geometry. All configurations share identical baseline dimensions, including the number of tubes, shell diameters, and lengths, with variations introduced only through baffle design to ensure fair comparison.

Turbulence Modelling

Turbulence effects are modelled using the standard k–ε model, where the transport equations for turbulent kinetic energy (k) and its dissipation rate (ε) are solved to account for turbulence-induced momentum and heat transfer enhancement.

Standard k–ε Model

In the present CFD analysis, turbulence effects are modelled using the standard k–ε turbulence model, which introduces two additional transport equations to account for the effects of turbulence on momentum and heat transfer.

Transport Equation for Turbulent Kinetic Energy (k)

International Journal of Engineering Research & Technology (IJERT)
ISSN: 2278-0181
Vol. 14 Issue 12 , December - 2025

$$\frac{\partial(\rho k)}{\partial t} + \nabla \cdot (\rho \mathrm{u} k) = \nabla \cdot \left[\left(\mu + \frac{\mu_t}{\sigma_k}\right) \nabla k\right] + G_k - \rho\varepsilon \quad (5)$$

where:

- k= turbulent kinetic energy (m²/s²)
- μ_t= turbulent (eddy) viscosity
- G_k= production of turbulent kinetic energy due to velocity gradients
- σ_k= turbulent Prandtl number for k

Transport Equation for Turbulent Dissipation Rate (ε)

$$\frac{\partial(\rho\varepsilon)}{\partial t} + \nabla \cdot (\rho \mathrm{u} \varepsilon) = \nabla \cdot \left[\left(\mu + \frac{\mu_t}{\sigma_\varepsilon}\right) \nabla \varepsilon\right] + C_{1\varepsilon} \frac{\varepsilon}{k} G_k - C_{2\varepsilon} \rho \frac{\varepsilon^2}{k} \quad (6)$$

where:

- ε= turbulent dissipation rate (m²/s³)
- σ_ε= turbulent Prandtl number for ε
- $C_{1\varepsilon}$, $C_{2\varepsilon}$= empirical model constants

Turbulent (Eddy) Viscosity

$$\mu_t = \rho C_\mu \frac{k^2}{\varepsilon} \quad (7)$$

Thermal performance parameters are evaluated from the CFD results using a limited set of objective-oriented equations. Heat exchanger effectiveness is calculated as the ratio of actual heat transfer rate to the maximum possible heat transfer rate. The overall heat transfer coefficient is determined using the heat transfer rate, tube-side outside heat transfer area, and the logarithmic mean temperature difference (LMTD). Shell-side heat transfer enhancement is further characterised using the Nusselt number to relate flow behaviour to thermal improvement. Pressure drop across the shell side and hydraulic diameter are also computed to support thermo-hydraulic interpretation, while the primary performance indicators remain effectiveness, overall heat transfer coefficient, outlet temperature, enhancement ratio, and LMTD.

Effectiveness: Effectiveness is the ratio of the actual heat transfer rate to the maximum possible heat transfer rate in a heat exchanger.

$$\varepsilon_f = \frac{q^{"}_{actual}}{q^{"}_{max}} \quad (8)$$

- ε_f = Heat exchanger effectiveness
- $q^{"}_{actual}$ = Actual heat transfer rate (W)
- $q^{"}_{max}$ = Maximum possible heat transfer rate (W)

Effectiveness (ε_f) → performance comparison with ideal heat exchanger

Maximum possible heat transfer

This occurs when the fluid with the minimum heat capacity rate undergoes the maximum temperature change.

$$q^{"}_{max} = C\left(T_{h,i} - T_{c,i}\right)_{min} \quad (9)$$

Actual heat transfer

$$q^{"}_{actual} = C_h\left(T_{h,i} - T_{h,o}\right) = C_c\left(T_{c,o} - T_{c,i}\right) \quad (10)$$

Heat capacity rate

$$C_h = \dot{m}_h C_{p,h} C_c = \dot{m}_c C_{p,c} \quad (11)$$

- C_h = Heat capacity rate of hot fluid (W/K)
- C_c = Heat capacity rate of cold fluid (W/K)
- C_{min} = Minimum of $C_h$and C_c
- $\dot{m}_h$ = Mass flow rate of hot fluid (kg/s)
- $\dot{m}_c$ = Mass flow rate of cold fluid (kg/s)

International Journal of Engineering Research & Technology (IJERT)
ISSN: 2278-0181
Vol. 14 Issue 12 , December - 2025

- $C_{p,h}$ = Specific heat of hot fluid (J/kg·K)
- $C_{p,c}$ = Specific heat of cold fluid (J/kg·K)

Final effectiveness expression

$$\varepsilon_f = \frac{C_h(T_{h,i}-T_{h,o})}{C(T_{h,i}-T_{c,i})_{min}} = \frac{C_c(T_{c,o}-T_{c,i})}{C_{min}(T_{h,i}-T_{c,i})} \quad (12)$$

- $T_{h,i}$ = Hot fluid inlet temperature
- $T_{h,o}$ = Hot fluid outlet temperature
- $T_{c,i}$ = Cold fluid inlet temperature
- $T_{c,o}$ = Cold fluid outlet temperature

High-resolution computational meshes comprising approximately 6.8–7.8 million cells are generated for each configuration. A grid-independence study is conducted using the hot-fluid outlet temperature as the monitoring parameter, confirming that variations become negligible beyond approximately 7.25 million cells; this mesh density is therefore adopted for all simulations. Boundary conditions are fixed across all cases, with hot water flowing through the tube side at 1 LPM and 50 °C, and cold water flowing through the shell side at 23 °C with volumetric flow rates of 2, 4, 6, and 8 LPM. Pressure outlets with zero-gauge pressure, no-slip wall conditions, and an adiabatic outer shell are applied. Model accuracy is validated by comparing predicted temperature contours with published results from A. Q. Najm et al. (2024). Following validation, the same numerical setup is consistently used for all baffle configurations, ensuring that observed performance variations are solely attributable to baffle geometry and shell-side flow rate.

Overall heat transfer coefficient

The overall heat transfer coefficient represents the combined resistance to heat transfer due to convection, conduction, and fouling.

$$U_o = \frac{Q}{A_0.\Delta T_{LMTD}} \quad (13)$$

- U_o = Overall heat transfer coefficient (W/m²·K)
- A_0 = Heat transfer area (m²)
- ΔT_{LMTD} = Log mean temperature difference (K)

Overall heat transfer coefficient (U) → actual heat transfer ability of the exchanger

Outside heat transfer area

$$A_0 = \pi d_0 L N_t \quad (14)$$

- d_0 = Outer diameter of tube (m)
- L =Tube length (m)
- N_t = Number of tubes

Average heat transfer rate

$$Q_{avg} = \frac{1}{2}(Q_h - Q_c) \quad (15)$$

- Q_{avg} = Average heat transfer rate (W)
- Q_h = Heat transfer rate from hot fluid (W)
- Q_c = Heat transfer rate to cold fluid (W)

(Used when small imbalance exists between hot-side and cold-side heat transfer due to numerical or experimental errors.)

Log Mean Temperature Difference (LMTD)

Applicable for counter-flow heat exchangers (same form used with appropriate temperature pairs for parallel flow).

$$\Delta T_{LMTD} = \frac{(T_{h,i}-T_{c,o})-(T_{h,o}-T_{c,i})}{\ln\left(\frac{(T_{h,i}-T_{c,o})}{(T_{h,o}-T_{c,i})}\right)} \quad (16)$$

The pressure drops across the shell and tube calculated as the difference between the inlet and outlet pressure.

International Journal of Engineering Research & Technology (IJERT)
ISSN: 2278-0181
Vol. 14 Issue 12 , December - 2025

The pressure drop is defined as the difference between the inlet and outlet pressures of the fluid flowing through either the shell side or tube side of a heat exchanger.

$$\Delta p = P_{in} - P_o \quad (17)$$

- Δp = Pressure drops in Pa
- P_{in} = Inlet pressure in Pa
- P_o = Outlet pressure in Pa

Hydraulic Diameter (Dh) — CALCULATION *[A. Q. Najm et al. (2024)]*

Parameter	Value
Shell diameter (large)	120 mm
Shell diameter (small)	110 mm
Tube OD	6.3 mm
Number of tubes	18

Mean shell diameter

$$D_{s,mean} = \frac{D_{large} + D_{small}}{2} = \frac{120+110}{2} = 115 \text{ mm} = 0.115 \text{ m} \quad (18)$$

Tube outer diameter

$$D_o = 6.3 \text{ mm} = 0.0063 \text{ m} \quad (19)$$

Shell cross-sectional area

$$A_{shell} = \frac{\pi}{4} D_{s,mean}^2 = \frac{\pi}{4}(0.115)^2 = 0.01038 \text{ m}^2 \quad (20)$$

Area blocked by tubes

$$A_{tubes} = N \cdot \frac{\pi}{4} D_o^2 \quad (21)$$

$$= 18 \cdot \frac{\pi}{4}(0.0063)^2 = 0.000561 \text{ m}^2 \quad (22)$$

Net shell-side flow area

$$A_{flow} = A_{shell} - A_{tubes} \quad (23)$$

$$= 0.01038 - 0.000561 = 0.00982 \text{ m}^2 \quad (24)$$

Wetted perimeter (tube outer surfaces)

$$P_{wetted} = N \cdot \pi D_o \quad (25)$$

$$= 18 \cdot \pi \cdot 0.0063 = 0.356 \text{ m} \quad (26)$$

Hydraulic diameter

$$D_h = \frac{4A_{flow}}{P_{wetted}} \quad (27)$$

$$D_h = \frac{4 \times 0.00982}{0.356} = 0.110 \text{ m} \quad (28)$$

Heat-transfer coefficient

$$h = \frac{Q}{A(T_w - T_b)} \text{ W/m}^2\text{K} \quad (29)$$

Cold side

$$T_{b,cold} = T_{cold,out} \quad (30)$$

Hot side

$$T_{b,hot} = T_{hot,out} \quad (31)$$

Nusselt Number

$$Nu = \frac{hD_h}{k} \quad (32)$$

International Journal of Engineering Research & Technology (IJERT)
ISSN: 2278-0181
Vol. 14 Issue 12 , December - 2025

V. RESULT AND DISCUSSION

A validated three-dimensional CFD model was successfully applied to analyse the thermal and flow behaviour of a shell-and-tube heat exchanger with four shell-side configurations: no baffle (Design-1), conventional wavy baffle (Design-2), proposed wavy-segmented baffle (Design-3), and proposed half-segmented spiral baffle (Design-4). Flow and temperature contours confirmed that the no-baffle configuration exhibits predominantly axial flow with weak turbulence and poor mixing, resulting in the lowest heat transfer performance. The introduction of baffles progressively intensified shell-side turbulence, improved cross-flow around the tube bundle, and enhanced thermal interaction between hot and cold fluids.

CFD Results at 8 LPM shell volumetric flow rate:

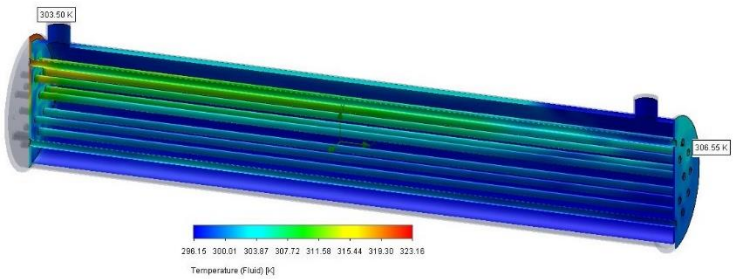

Fig. 2: Temperature Distribution of fluid inside the shell and tube heat exchanger without baffle at 8 LPM

Fig.2 illustrates the CFD-predicted temperature distribution of the shell-side fluid in a shell-and-tube heat exchanger without baffles (Design-1) operating at a shell volumetric flow rate of 8 LPM. The contour plot shows variation fluid temperature from the cold fluid outlet (~303.5 K) to the hot fluid outlet (~306.55 K), confirming continuous heat transfer from the shell-side fluid to the tube-side fluid along the exchanger length.

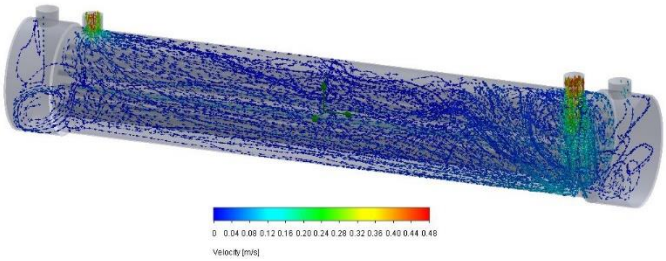

Fig. 3: Velocity Distribution of fluid inside the shell and tube heat exchanger without baffle at 8 LPM

Fig.3 presents the velocity distribution and flow streamlines of the shell-side fluid in the shell-and-tube heat exchanger without baffles (Design-1) at a shell volumetric flow rate of 8 LPM. The streamline plot indicates that the shell-side fluid predominantly follows an axial flow path from inlet to outlet, with higher velocities concentrated near the inlet and outlet nozzles (up to ~0.48 m/s) due to flow acceleration caused by sudden area changes.

CFD Results at 8 LPM shell volumetric flow rate:

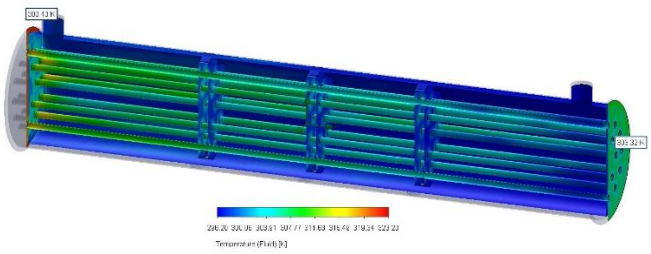

Fig. 4: Temperature Distribution of fluid inside the shell and tube heat exchanger with wavy baffle at 8 LPM

Fig. 4 illustrates the CFD-predicted temperature distribution of the shell-side fluid in a shell-and-tube heat exchanger with wavy baffles (Design-2) operating at a shell volumetric flow rate of 8 LPM. The contour plot shows variation fluid temperature from the cold fluid outlet (~300.43 K) to the hot fluid outlet (~303.32 K), confirming continuous heat transfer from the shell-side fluid to the tube-side fluid along the exchanger length.

International Journal of Engineering Research & Technology (IJERT)
ISSN: 2278-0181
Vol. 14 Issue 12 , December - 2025

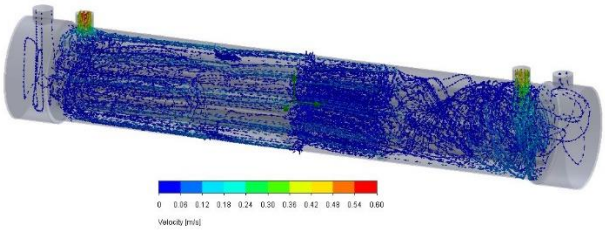

Fig. 5: Velocity Distribution of fluid inside the shell and tube heat exchanger with wavy baffle at 8 LPM

Fig. 5 presents the velocity distribution and flow streamlines of the shell-side fluid in the shell-and-tube heat exchanger with wavy baffles (Design-2) at a shell volumetric flow rate of 8 LPM. The streamline plot indicates that the shell-side fluid predominantly follows an axial flow path from inlet to outlet, with higher velocities concentrated near the inlet and outlet nozzles (up to ~0.6 m/s) due to flow acceleration caused by sudden area changes.

CFD Results at 8 LPM shell volumetric flow rate:

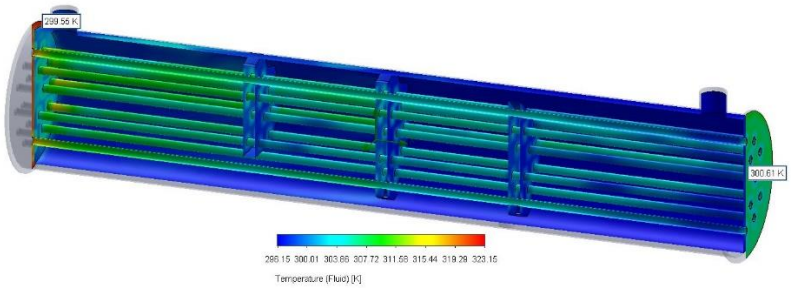

Fig. 6: Temperature Distribution of fluid inside the shell and tube heat exchanger with wavy segmental baffle at 8 LPM

Fig. 6 illustrates the CFD-predicted temperature distribution of the shell-side fluid in a shell-and-tube heat exchanger with wavy segmental baffles (Design-3) operating at a shell volumetric flow rate of 8 LPM. The contour plot shows variation fluid temperature from the cold fluid outlet (~299.55 K) to the hot fluid outlet (~300.61 K), confirming continuous heat transfer from the shell-side fluid to the tube-side fluid along the exchanger length.

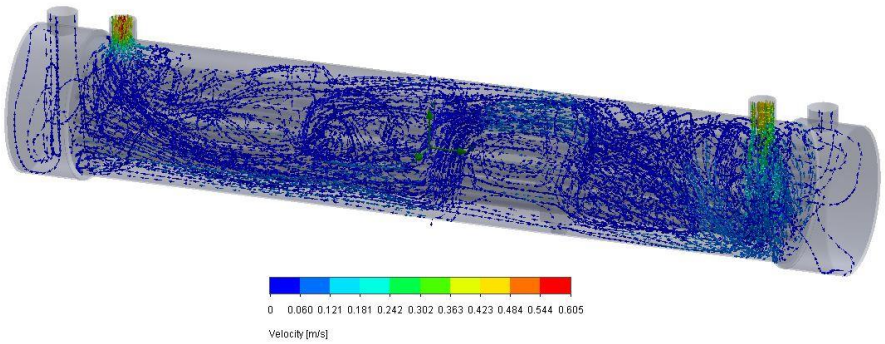

Fig. 7: Velocity Distribution of fluid inside the shell and tube heat exchanger with wavy segmental baffle at 8 LPM

Fig. 7 presents the velocity distribution and flow streamlines of the shell-side fluid in the shell-and-tube heat exchanger with wavy segmental baffles (Design-3) at a shell volumetric flow rate of 8 LPM. The streamline plot indicates that the shell-side fluid predominantly follows an axial flow path from inlet to outlet, with higher velocities concentrated near the inlet and outlet nozzles (up to ~0.605 m/s) due to flow acceleration caused by sudden area changes.

CFD Results at 8 LPM shell volumetric flow rate:

International Journal of Engineering Research & Technology (IJERT)
ISSN: 2278-0181
Vol. 14 Issue 12 , December - 2025

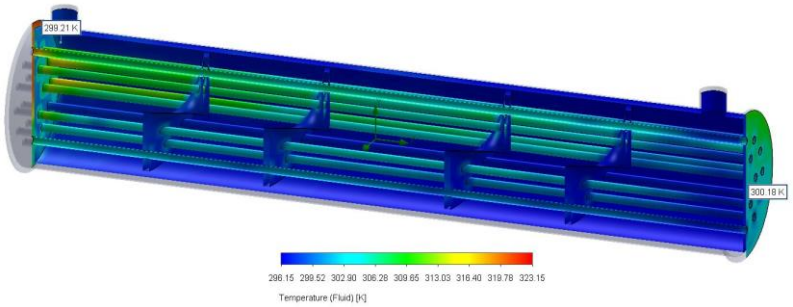

Fig. 8: Temperature Distribution of fluid inside the shell and tube heat exchanger with half-segmented spiral baffle at 8 LPM

Fig. 8 illustrates the CFD-predicted temperature distribution of the shell-side fluid in a shell-and-tube heat exchanger with half-segmented spiral baffles (Design-4) operating at a shell volumetric flow rate of 8 LPM. The contour plot shows variation fluid temperature from the cold fluid outlet (~299.21 K) to the hot fluid outlet (~300.18 K), confirming continuous heat transfer from the shell-side fluid to the tube-side fluid along the exchanger length.

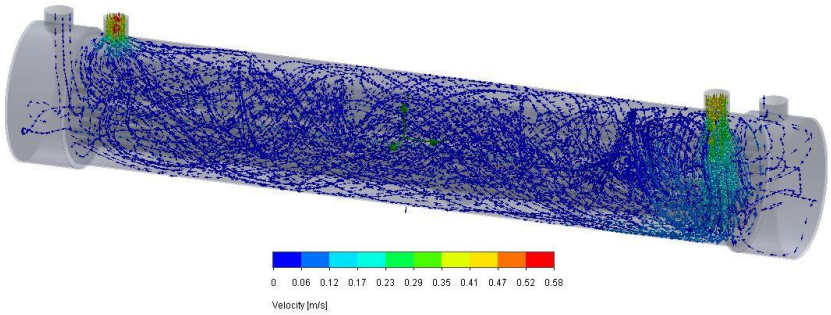

Fig. 9: Velocity Distribution of fluid inside the shell and tube heat exchanger with half-segmented spiral baffle at 8 LPM

Fig. 9 presents the velocity distribution and flow streamlines of the shell-side fluid in the shell-and-tube heat exchanger with half-segmented spiral baffles (Design-4) at a shell volumetric flow rate of 8 LPM. The streamline plot indicates that the shell-side fluid predominantly follows an axial flow path from inlet to outlet, with higher velocities concentrated near the inlet and outlet nozzles (up to ~0.58 m/s) due to flow acceleration caused by sudden area changes.

Quantitative results show that increasing shell-side volumetric flow rate from 2 to 8 LPM enhances heat transfer for all configurations; however, the magnitude of improvement strongly depends on baffle geometry. Compared to the no-baffle case, the conventional wavy baffle provides moderate enhancement, while the proposed designs yield substantially higher performance. At 8 LPM, the hot-fluid outlet temperature decreases by approximately 22% for Design-4 compared to 11% for Design-1, indicating superior heat removal. Shell-side velocities increase nearly linearly with flow rate, with Design-4 achieving up to 20–25% higher velocities than the no-baffle case, demonstrating stronger turbulence generation and reduced stagnant zones.

International Journal of Engineering Research & Technology (IJERT)
ISSN: 2278-0181
Vol. 14 Issue 12 , December - 2025

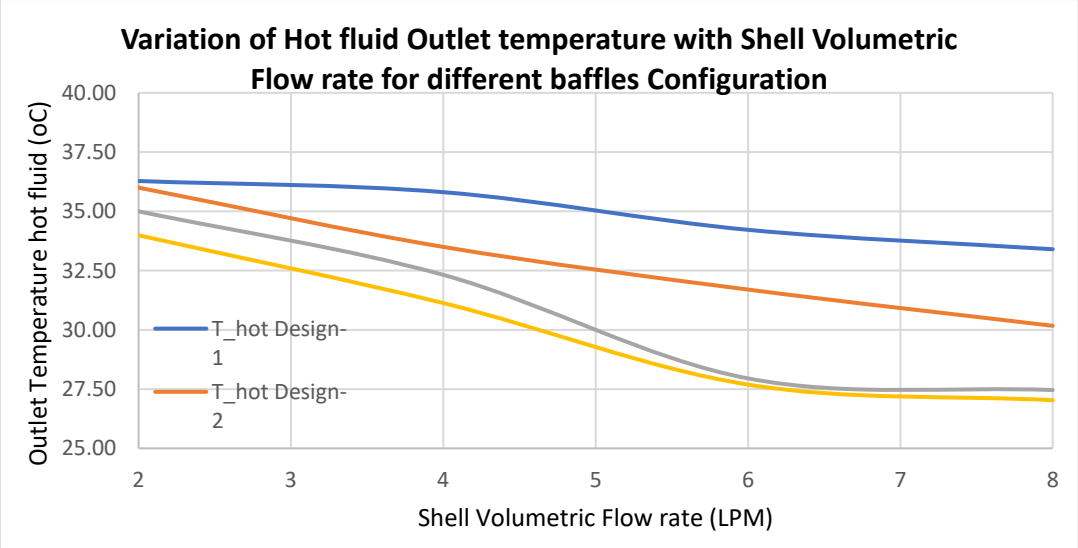

Fig. 10: Variation of Hot fluid Outlet temperature with Shell Volumetric Flow rate for different baffles Configuration

Fig. 10 shows that the hot fluid outlet temperature decreases monotonically with increasing shell volumetric flow rate for all baffle configurations, indicating enhanced heat removal at higher flow rates. For Design-1, the outlet temperature drops from about 38 °C at 2 LPM to nearly 34 °C at 8 LPM, corresponding to a reduction of approximately 11%, which is the smallest decrease. Design-2 shows a decrease from around 36 °C to 30 °C, giving nearly 17% reduction. Design-3 exhibits a stronger decline from about 35 °C to nearly 27.5 °C, resulting in approximately 21% reduction. Design-4 provides the maximum cooling effect, with outlet temperature decreasing from around 34 °C to about 26.5 °C, corresponding to roughly 22% reduction. The larger temperature drop in advanced baffle designs indicates improved turbulence, higher heat transfer rates, and better thermal performance compared to the conventional configuration.

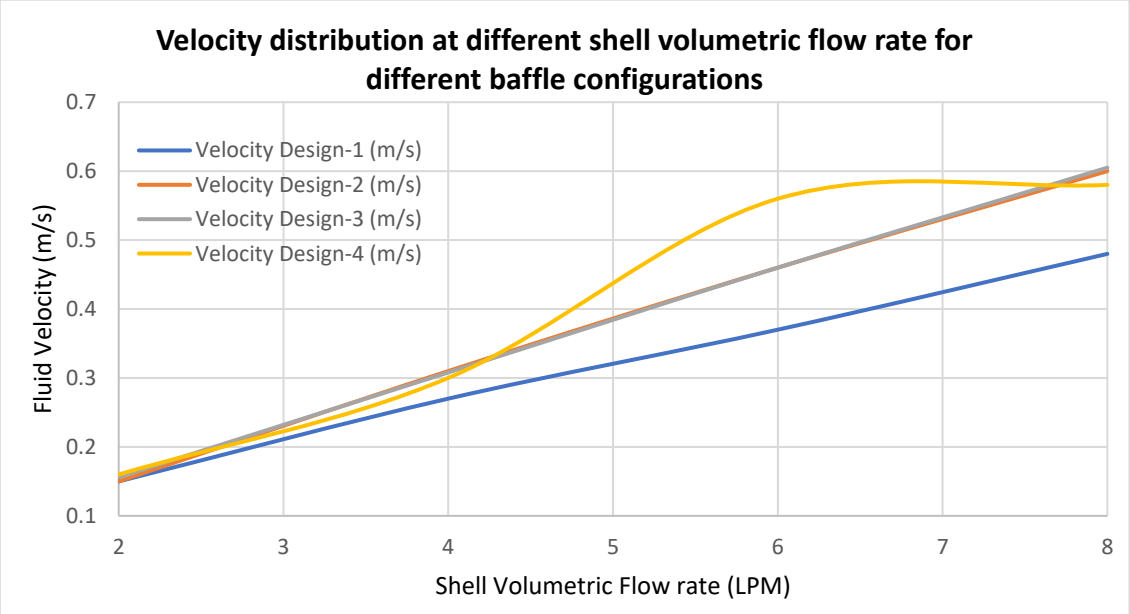

Fig. 11: Velocity distribution at different shell volumetric flow rate for different baffle configurations

Fig. 11 illustrates the variation of shell-side fluid velocity with shell volumetric flow rate for different baffle configurations (Design-1 to Design-4). For all designs, the velocity increases monotonically with increasing flow rate from 2 to 8 LPM, indicating a direct dependence of flow momentum on the imposed volumetric flow. Design-1 consistently exhibits the lowest velocity across the entire range, reflecting weaker flow guidance and limited obstruction, whereas Designs-2 and-3 show moderate and nearly linear velocity enhancement due to improved redirection of the shell-side flow. Design-4 demonstrates the highest velocity at intermediate and higher flow rates, with a pronounced rise beyond 4 LPM, signifying stronger flow acceleration and enhanced turbulence generation induced by the optimized baffle arrangement. At 8 LPM, the shell-side velocity in Design-4 is approximately 20–25% higher than

International Journal of Engineering Research & Technology (IJERT)
ISSN: 2278-0181
Vol. 14 Issue 12 , December - 2025

that of Design-1, while Designs-2 and-3 maintain intermediate values. This trend confirms that effective baffle configuration significantly intensifies shell-side flow velocity, thereby promoting improved convective heat transfer performance with increasing shell volumetric flow rate.

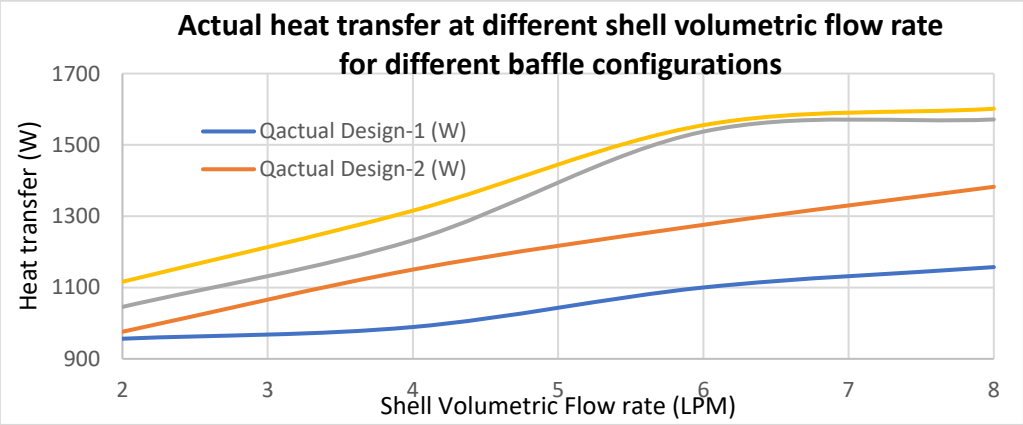

Fig. 12: Actual heat transfer at different shell volumetric flow rate for different baffle configurations

The CFD-predicted actual heat transfer results clearly demonstrate the progressive enhancement in thermal performance with the incorporation of advanced baffle configurations over the investigated shell-side volumetric flow rate range of 2–8 LPM. For the baseline design without baffles (Design-1), the actual heat transfer increases from 956.48 W at 2 LPM to 1157.25 W at 8 LPM, primarily due to increased convective transport with higher flow rate. Relative to Design-1, the wavy baffle configuration (Design-2) exhibits a moderate improvement, with heat transfer enhancement of approximately 2.0% at 2 LPM, which increases significantly to about 16.3%, 15.9%, and 19.4% at 4, 6, and 8 LPM, respectively, indicating effective flow redirection and turbulence promotion at higher flow rates. The segmental wavy baffle (Design-3) provides a substantially higher enhancement, achieving an increase of nearly 9.3% at 2 LPM and rising sharply to about 24.6% at 4 LPM, 39.7% at 6 LPM, and 35.8% at 8 LPM compared to the no-baffle configuration, due to repeated disruption of thermal boundary layers and improved shell-side fluid mixing. The half segmental spiral baffle (Design-4) delivers the maximum heat transfer augmentation among all designs, with improvements of approximately 16.7% at 2 LPM, 33.0% at 4 LPM, 41.4% at 6 LPM, and 38.3% at 8 LPM relative to Design-1, which can be attributed to the continuous spiral flow path that minimizes bypass flow and maintains sustained turbulence along the tube bundle.

Thermal performance parameters further confirm the superiority of advanced baffle configurations. The shell-side heat-transfer coefficient increases by up to 232%, and the Nusselt number by ~232%, for the half-segmented spiral baffle relative to the baseline configuration at high flow rates. Effectiveness rises from 0.51–0.61 (Design-1) to a maximum of 0.85 (Design-4), while the enhancement ratio reaches 1.38, indicating nearly 38% improvement in thermal performance. A consistent reduction in LMTD for advanced designs reflects more effective heat transfer achieved with a lower thermal driving force.

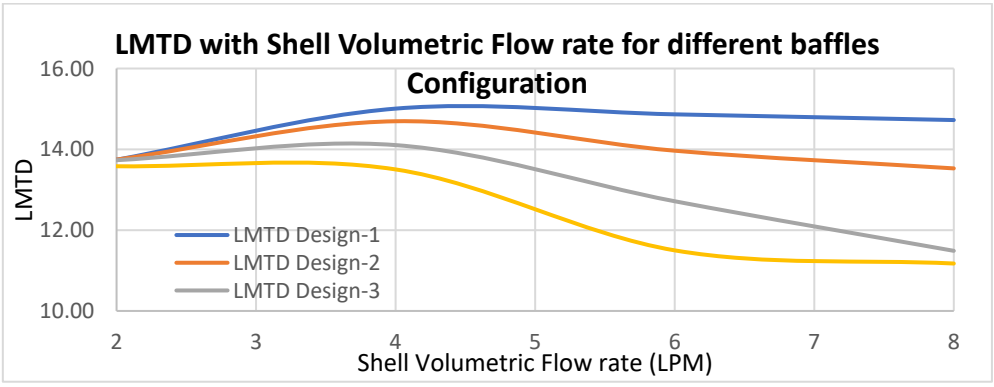

Fig. 13: LMTD with Shell Volumetric Flow rate for different baffles Configuration

The variation of logarithmic mean temperature difference (LMTD) with shell-side volumetric flow rate provides important insight into the thermal driving force under different baffle configurations. Considering Design-2 (wavy baffle) as the base design adopted from literature, the LMTD values indicate how enhanced convection alters the temperature profiles within the heat exchanger. At 2 LPM, Design-2 shows a slightly higher LMTD (13.75 K) than Design-1 (13.29 K), corresponding to an increase of approximately 3.5%, due to moderate improvement in shell-side mixing. However, as the flow rate increases, Design-2 exhibits a gradual reduction

International Journal of Engineering Research & Technology (IJERT)
ISSN: 2278-0181
Vol. 14 Issue 12 , December - 2025

in LMTD compared to Design-1, with decreases of about 2.0% at 4 LPM, 5.0% at 6 LPM, and 7.3% at 8 LPM, indicating more effective heat transfer that reduces the overall temperature difference requirement. Compared to the base design, the segmental wavy baffle (Design-3) shows marginal change at 2 LPM (−0.15%) but a significant reduction in LMTD of approximately 4.0%, 15.1%, and 14.8% at 4, 6, and 8 LPM, respectively, reflecting stronger turbulence and enhanced thermal interaction. The half segmental spiral baffle (Design-4) exhibits the maximum reduction in LMTD across all operating conditions, with decreases of about 1.0% at 2 LPM, 8.1% at 4 LPM, 17.7% at 6 LPM, and 17.1% at 8 LPM relative to the base design, owing to its continuous spiral flow path that ensures uniform temperature gradients and superior heat transfer effectiveness. Overall, the progressive reduction in LMTD from Design-2 to Design-4 confirms that advanced baffle geometries achieve higher heat transfer rates while requiring a lower thermal driving force, with Design-4 identified as the most thermally efficient configuration, followed by Design-3, Design-2, and Design-1.

Overall comparison across all performance metrics effectiveness, overall heat-transfer coefficient, enhancement ratio, outlet temperatures, and LMTD identifies the half-segmented spiral baffle (Design-4) as the optimal configuration, followed closely by the wavy-segmented baffle (Design-3). The conventional wavy baffle offers only moderate improvement, while the no-baffle design consistently performs worst. The results clearly demonstrate that optimized baffle geometry, combined with higher shell-side flow rates, significantly enhances shell-side heat transfer, validating the proposed designs as effective solutions for high-performance shell-and-tube heat exchangers.

VI. CONCLUSION

A comprehensive CFD-based investigation was conducted to evaluate the impact of baffle geometry and shell-side flow rate on the thermal performance of a shell-and-tube heat exchanger. The results clearly indicate that the no-baffle configuration yields the lowest heat transfer performance due to weak turbulence and poor flow mixing, while the conventional wavy baffle provides only moderate improvement. In contrast, the proposed wavy-segmented and half-segmented spiral baffles significantly enhance shell-side turbulence, leading to higher heat transfer coefficients, increased effectiveness, reduced outlet temperatures, and lower LMTD values across all operating conditions. Among the configurations studied, the half-segmented spiral baffle demonstrates the best overall thermo-hydraulic performance, achieving up to 38% enhancement ratio and the highest effectiveness. The study confirms that strategic modification of baffle geometry, combined with higher shell-side flow rates, is an effective approach for improving shell-side heat transfer and overall exchanger efficiency, making the proposed designs promising for advanced industrial heat exchanger applications.

REFERENCES

[1] Syed Maaz Hasan et al. (2025) Performance enhancement of a shell-and-tube heat exchanger using a novel baffle design, Case Studies in Thermal Engineering, Volume 74, October 2025, 106800.https://doi.org/10.1016/j.csite.2025.106800.
[2] Huy Minh Khoi Hoang et al. (2025) A novel shell-and-tube heat exchanger design with alternative inclined baffles, Case Studies in Thermal Engineering Volume 65, January 2025, 105542.https://doi.org/10.1016/j.csite.2024.105542.
[3] Muhammad Waleed et al. (2025) Numerical analysis of shell and tube heat exchanger with combination of different baffles, Case Studies in Thermal Engineering Volume 65, January 2025, 105658.https://doi.org/10.1016/j.csite.2024.105658.
[4] Zhengfeng Shuai et al. (2025) Thermal performance of condensation phase change in the shell side of discontinuous helical baffle heat exchanger, Case Studies in Thermal Engineering Volume 68, April 2025, 105959. https://doi.org/10.1016/j.csite.2025.105959.
[5] Bailey Spickler et al. (2025) Surface roughness and dimensional evaluation of laser powder bed fusion additively manufactured shell and tube heat exchangers, Thermal Science and Engineering Progress Volume 65, September 2025, 103858. https://doi.org/10.1016/j.tsep.2025.103858.
[6] D. Pardillos-Pobo et al. (2025) Superheater-reheater integration in a one-shell coil-wound heat exchanger: analytical thermo-economic design for CSP, Applied Thermal Engineering Volume 279, Part B, 15 November 2025, 127632. https://doi.org/10.1016/j.applthermaleng.2025.127632.
[7] Yuyang Yuan et al. (2024) Numerical simulation and multi-objective optimization design of conjugate heat transfer in novel double shell-passes multi-layer helically coiled tubes heat exchangers, Case Studies in Thermal Engineering Volume 62, October 2024, 105155. https://doi.org/10.1016/j.csite.2024.105155.
[8] Zhe Xu et al. (2023) Design optimization of a shell-and-tube heat exchanger with disc-and-doughnut baffles for aero-engine using one hybrid method of NSGA II and MOPSO, Case Studies in Thermal Engineering Volume 41, January 2023, 102644. https://doi.org/10.1016/j.csite.2022.102644.
[9] Mehmet Akif kartal et al. (2023) Numerical analysis of multipurpose shell-tube-heat exchanger withal stylized geometry at different baffle gaps and various flow rates, Case Studies in Thermal Engineering Volume 52, December 2023, 103810. https://doi.org/10.1016/j.csite.2023.103810.
[10] Quanyu Gong et al. (2023) Experimental and numerical exploration on improved heat transfer by continuous spiral flow in shell of spiral wound corrugated tube heat exchanger, Case Studies in Thermal Engineering Volume 51, November 2023, 103483. https://doi.org/10.1016/j.csite.2023.103483.
[11] Qipeng Li et al. (2023) Investigation of noncircular orifice supporting baffle longitudinal flow heat exchangers, Case Studies in Thermal Engineering Volume 47, July 2023, 103104. https://doi.org/10.1016/j.csite.2023.103104.
[12] Sh. Asadbeigi et al. (2023) Analyzing and simulating heat transfer and designing a shell and tube heat exchanger for the pasteurization process of tomato paste: A CFD study, Heliyon Volume 9, Issue 11, November 2023, e21593. https://doi.org/10.1016/j.heliyon.2023.e21593.
[13] Mohammad Ramin Daneshparvar et al. (2022) Multi-objective optimization of helical baffles in the shell-and-tube heat exchanger by computational fluid dynamics and genetic algorithm, Energy Reports Volume 8, November 2022, Pages 11064-11077. https://doi.org/10.1016/j.egyr.2022.08.249.
[14] Marwa Ben Slimene et al. (2022) Numerical investigation of the flow dynamics and heat transfer in a rectangular shell-and-tube heat exchanger, Case Studies in Thermal Engineering Volume 32, April 2022, 101873. https://doi.org/10.1016/j.csite.2022.101873.